

**Extreme weather events in early Summer 2018 connected by a  
recurrent hemispheric wave pattern.**

**Kai Kornhuber<sup>1,2</sup>, Scott Osprey<sup>1,2</sup>, Dim Coumou<sup>3,4</sup>, Stefan Petri<sup>3</sup>,  
Vladimir Petoukhov<sup>3</sup>, Stefan Rahmstorf<sup>3</sup>, Lesley Gray<sup>1,2</sup>**

<sup>1</sup>Atmospheric, Oceanic and Planetary Physics, University of Oxford, Oxford, United Kingdom

<sup>2</sup>National Centre for Atmospheric Science, United Kingdom

<sup>3</sup>Earth System Analysis, Potsdam Institute for Climate Impact Research, Potsdam, Germany

<sup>4</sup>Institute for Environmental Studies, Vrije Universiteit Amsterdam, Amsterdam, Netherlands

Corresponding author: Kai Kornhuber (kai.kornhuber@physics.ox.ac.uk)

**Key Points:**

- We identify a recurrent Rossby-wave 7 teleconnection in Northern Hemisphere summer that exhibits a fixed phase position.
- It has been observed during summers that featured extreme heat-waves in Central US, Western Europe and the Caspian Sea region.
- This teleconnection was related to several regional weather extremes occurring near simultaneously across the mid-latitudes in June-July 2018.

## 1 Abstract

2 The summer of 2018 witnessed a number of extreme weather events such as heatwaves in  
3 North America, Western Europe and the Caspian Sea region and rainfall extremes in South-  
4 East Europe and Japan that occurred near-simultaneously. Here we show that these extremes  
5 were connected by an amplified hemisphere-wide wavenumber 7 circulation pattern. We  
6 show that this pattern constitutes a teleconnection in Northern Hemisphere summer associated  
7 with prolonged and above-normal temperatures in North America, Western Europe and the  
8 Caspian Sea region. This pattern was also observed during the European heatwaves of 2003,  
9 2006, 2012 and 2015 among others. We show that the occurrence of this wave 7 pattern has  
10 increased over recent decades.

## 11 Plain Language Summary

12 During late June through to July 2018 a prolonged circumpolar circulation pattern linked  
13 weather extremes in North America, Western Europe, the Caspian Sea and Japan. We identified  
14 this pattern be a recurrent teleconnection pattern leading to heat extremes in specific regions,  
15 also observed during several other extreme summers.

## 16 1 Introduction

17 Boreal summer of 2018 saw several record breaking and persistent heat and rainfall extremes  
18 occurring simultaneously in the Northern Hemisphere (NH) mid-latitudes. In North America,  
19 Los Angeles and Montreal all-time high temperature records were set early in July leading to  
20 power outages and severe heat stress. In Western Europe, the UK experienced a record long  
21 drought and heat for 40 days lasting from mid-June to mid-July (1, 2). In Glasgow and Belfast  
22 all-time record temperatures were measured on June 28 (32°C, 29.5°C) and the ongoing  
23 drought conditions triggered water restrictions. Meanwhile, in Georgia and Yerevan record  
24 temperatures above 40°C were measured (also see areas witnessing record breaking  
25 temperatures in Fig. S2b). Further, heavy rainfall over Greece, Romania, Ukraine and  
26 Bulgaria at the end of June led to severe flooding damage (3). Early July extreme rainfall over  
27 Japan caused landslides and flooding (1) killing at least 120 people (also see section:  
28 *Japanese Floods* and Fig. S1 in Supplementary Materials).

## 29 2 Materials and Methods

30 Linear regression of the time-series shown in Fig. 4 C, D of the manuscript was done using a  
31 least-square fitting algorithm. Significance was defined at the 95% confidence level.

32 The surface temperature composite anomaly field (Fig 4. A, B) was determined from weekly  
33 temperature anomaly fields based on grid-point-wise detrended daily surface temperature  
34 fields from NCEP.NCAR. Significance was determined by comparing high amplitude events  
35 ( $>1.5\sigma$ ) with the mean of all remaining weeks using a t-test and an adjusted p-value  
36 determined by false discovery rate testing (FDR)(2).

37 Spectral decomposition of weekly averaged meridional wind at 300mb and orography fields  
38 into their basic components and phases (Fig. 3, Fig. 4) was done using a fast fourier  
39 transformation applied on their mid-latitudinal average 37.5° N – 57.5° N (3).

40 Phase velocities shown in Fig. 2e were determined from by taking a fourth-order accurate  
 41 numerical approximation of the transient derivative of its phase based on daily data following  
 42 Coumou et al. 2014 (3). In a second step 15-day running mean values of these daily phase  
 43 velocities are calculated.

### 44 3 Data

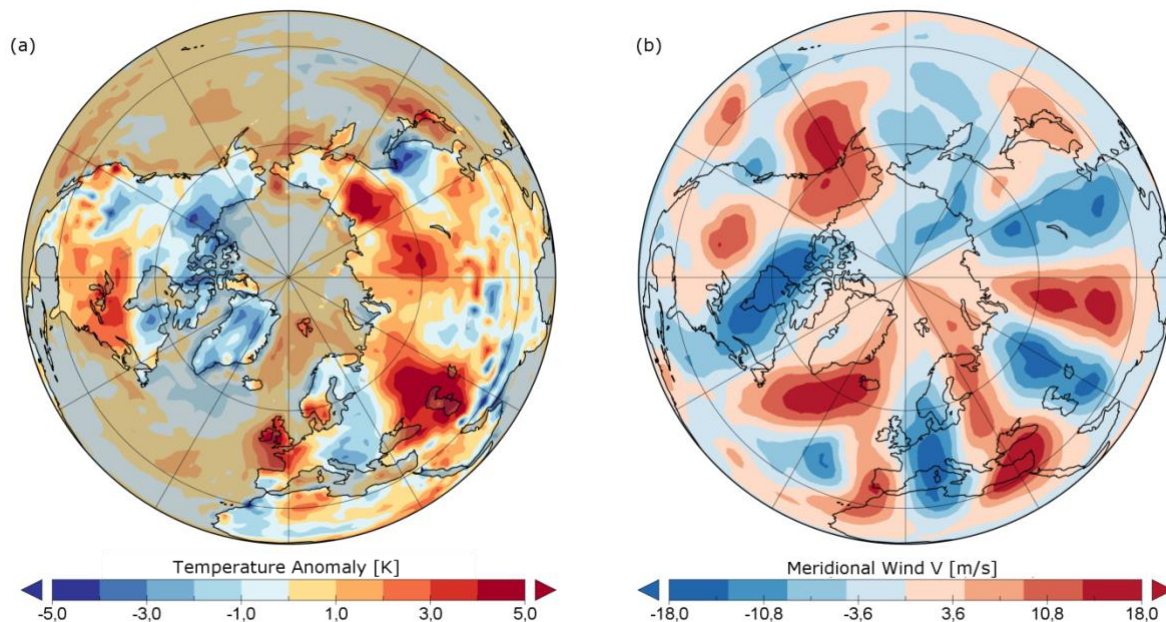
45 Daily wind and temperature data were taken from the archives of the European Center for  
 46 Medium Range Weather Forecasts (ECMWF) and the National Oceanic and Atmospheric  
 47 Administration (NOAA, NCEP-NCAR reanalysis (1)). In order to avoid spurious trends due  
 48 to changes in measurement systems we limited the analysis to the satellite based period (1979  
 49 – 2018).

### 50 4 Results

51 Here we show that these devastating extreme weather events were linked by a hemispheric-  
 52 scale circulation pattern, characterized by a strongly meandering wave-like jet-stream  
 53 stretching across the entire hemisphere (between  $\sim 30\text{-}60^\circ\text{N}$  in Fig. 1b). This wave-like  
 54 structure created alternating patterns of anomalously warm and cold conditions, setting the  
 55 stage for hot-dry extremes and persistent rain throughout the mid-latitudes (Fig. 1a, also see  
 56 Fig. S2). The circulation regime of summer 2018 was remarkable, not only in terms of the  
 57 amplitude and regularity of the wave-pattern but also due to its persistence, lasting for about  
 58 2-3 weeks from late-June to early-July.

59

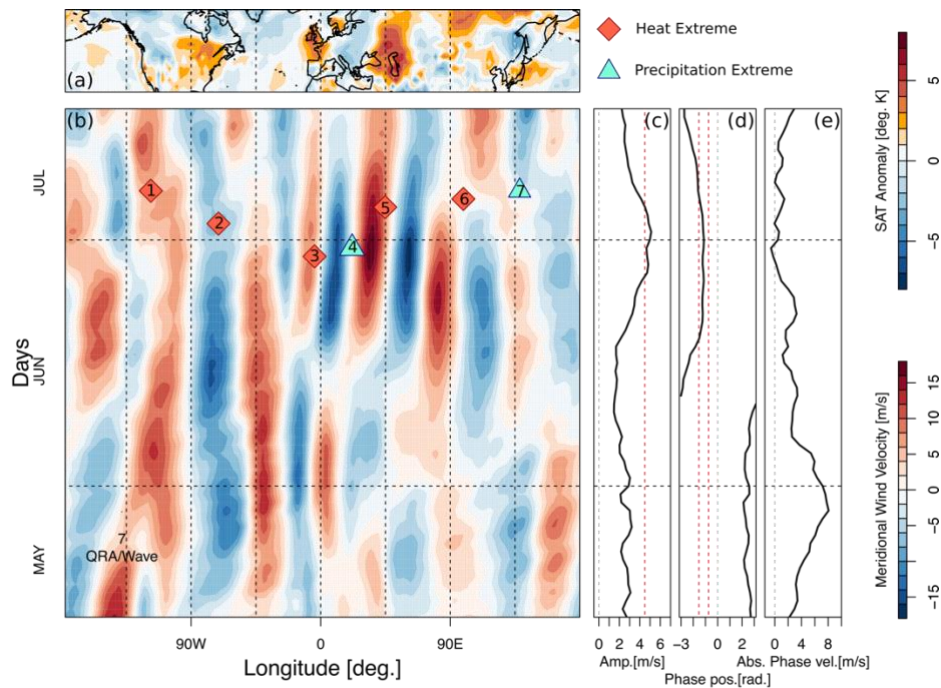
60



61

62 **Figure 1. Northern Hemisphere temperature anomalies and stationary Rossby wave**  
 63 **pattern in early July. (a)** Surface temperature Anomalies (from 1981-2010 climatology; 15-  
 64 day mean, centered on July 1<sup>st</sup> 2018). Oceans are masked in transparent grey. **(b)** As (A) but  
 65 for meridional wind V ( $\text{m s}^{-1}$ ) in the upper troposphere (250 mb).

66 This strongly meandering circulation regime created the necessary background conditions for  
 67 many simultaneous weather extremes. Figure 2b shows the onset and persistence of the wave  
 68 pattern as a Hovmöller plot (longitude vs. time) of the meridional winds averaged over the  
 69 mid-latitudes ( $37.5^{\circ}\text{N}$ - $57.5^{\circ}\text{N}$ , with the timing and longitudinal location of notable extreme  
 70 weather events superimposed. Starting at the end of June, a quasi-stationary wavenumber 7  
 71 (wave 7 from hereon) circulation pattern evolves (Fig. S3a,b), with large amplitude (Fig. 2b,  
 72 c, Fig.S3c), near-stationary phase position (Fig. 2d) and near-zero phase speed (Fig. 2e). The  
 73 amplitude starts to increase from mid-June, exceeding the 1.5 standard deviation threshold by  
 74 the end of June (Fig. 2c) and persists at that high level until early July. In concert with the  
 75 rising amplitude, the wave phase-shifts into a preferred position where it persists (indicated by  
 76 the dashed red lines in Fig. 2D, also see Fig. S4). The absolute phase speed of wave 7 slows  
 77 down at the moment when the preferred phase position is reached. Coinciding with the peak  
 78 of the stationary pattern from end of June to early July several heat and rainfall extremes  
 79 occur in the mid-latitudes (Fig. 2b, Fig. S2b).  
 80



81

82 **Figure 2. Time evolution of persistent wave 7 circulation pattern.** (a) NH surface air  
 83 temperatures (15-day mean centered on July 1<sup>st</sup> 2018). (b) Hovmöller (longitude-time) time  
 84 evolution of the mid. latitude (averaged over  $37.5^{\circ}\text{N}$  –  $57.5^{\circ}\text{N}$ ) meridional winds. A stationary  
 85 wave 7 pattern evolves in mid. June. The location and timing of extreme events are marked as  
 86 orange diamond (heat extreme) and blue triangle (precipitation extreme); from left to right: (1)  
 87 Los Angeles, (2) Montreal, (3) Belfast, (4) Sofia, (5) Tiflis, (6) Siberia, (7) Hiroshima. (c)  
 88 Amplitude of wave 7 ( $\text{m s}^{-1}$ ). The amplitude increases and exceeds 1.5 std (red dashed line)  
 89 at end of June shortly before heat records are broken across the mid-latitudes (also see Fig. S2b).  
 90 (d) Phase of wave 7 (radians). The phase becomes locked within its preferred position (marked  
 91 by red dashed lines) by mid-June. (e) Phase speed of wave 7 ( $\text{m s}^{-1}$ ). The phase speed slows  
 92 down in concert with the increasing amplitude and the phase locking of wavenumber 7.

93 Here we show that wave 7 is of particular importance, as it shows some unique behavior in  
94 that it tends to get locked in a specific preferred phase position as the amplitude increases and  
95 remain there for an extended period (4) (also see Fig. S4), constituting circumglobal  
96 teleconnection pattern in NH Summer. This is consistent with the work from Branstator et al.  
97 (5) who showed that zonally elongated zonal winds (see Fig. S9) can act as waveguides for  
98 planetary waves leading to co-variability in far-away regions (6).

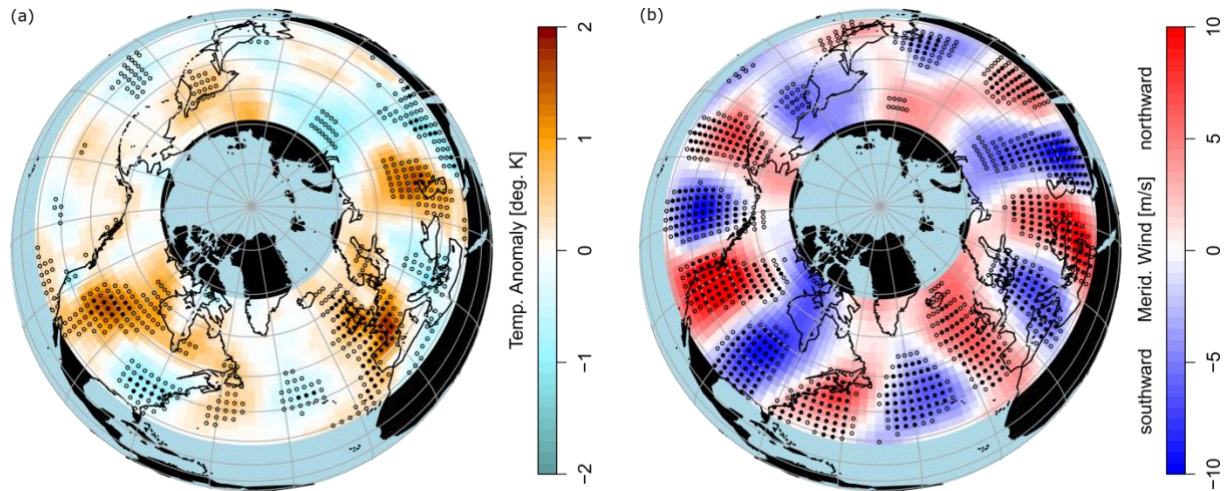
99

100 The hemispheric circulation exhibits spatially confined troughs and ridges which then persist  
101 over specific regions (Fig.3b) (4, 7). A characteristic circumglobal pattern of alternating  
102 temperature anomalies thus arises across the mid-latitudinal belt with significantly elevated  
103 surface temperatures over central North America, Western/Central Europe and the Caspian  
104 Sea region (Fig. 3a), just as observed in summer 2018 (Fig. 1a, Fig. 2a). Here, high amplitude  
105 wave 7 events were defined by weeks in JJA exceeding  $1.5\sigma$  (the pattern however is  
106 independent on the exact choice of threshold; see Fig. S5). In the regions identified above,  
107 dynamic contributions from the wave 7 circumglobal teleconnection can then intensify the  
108 normal summer temperatures and lead to heat waves on weekly to monthly time scales.  
109 In agreement, many of high amplitude wave 7 events coincide with heat extremes in Central  
110 North America and central Western Europe and the Caspian Sea region as suggested by the  
111 surface temperature anomaly map (Fig. 3a), among them the devastating heatwaves of 2003,  
112 2006, 2012 and 2015 (4, 8) (also see Fig. S6, Table S1).

113

114 Over recent decades the number of wave 7 *phase-locked* events (here defined as weeks with  
115 above average wave 7 amplitude within its preferred position, see Fig. S3) have increased  
116 significantly (0.95 confidence interval (Fig. 4b). Summers with more than one subsequent  
117 week of wave 7 phase-locked events did not occur prior to 1999, but since then have occurred  
118 at an increasing frequency (Table S1). This can be interpreted as an increase in persistence of  
119 such situations. In fact, the average number has doubled from about one to two weeks per  
120 year, while the number of years with more than two events per summer shows an almost  
121 eight-fold increase. Although the sign of the trend is independent of the applied amplitude  
122 threshold, the significance of the trend depends on the amplitude threshold, possibly due to  
123 the consequent reduction in ensemble size (Fig. 4b). The number of wave 7 events (weeks  
124 exceeding a specific wave amplitude threshold) show increasing but not significant trends  
125 independent of threshold applied (Fig. 4a). A significant trend for the amplitude of wave 7 in  
126 summer is only found when including data beyond the satellite measurement period (Fig. S7).  
127 In general, these trends should be treated cautiously as the period of satellite observations  
128 (1979 onwards) is relatively short and they might thus reflect multi-decadal oscillations in the  
129 earth system.

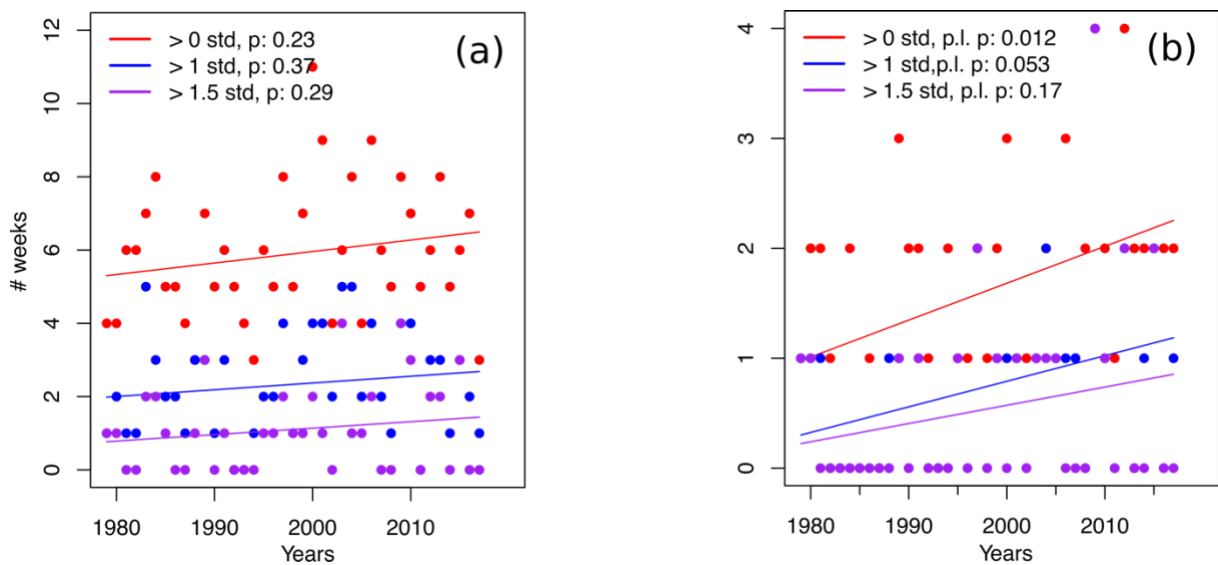
130



131

132 **Figure 3. A recurrent circumglobal wave 7 teleconnection.** (a) Composite plot of surface  
 133 temperature anomalies over the NH mid-latitudes ( $30^{\circ}\text{N} - 67.5^{\circ}\text{N}$ ) during weeks of high wave  
 134 7 amplitudes ( $>1.5\sigma$ ,  $N: 40$  weeks) in summer (JJA) over the NH mid-latitudes ( $30^{\circ}\text{N} - 67.5^{\circ}\text{N}$ )  
 135 observed over the period 1979 - 2016. (b) Meridional wind speeds (northward: red; southward:  
 136 blue) during those events. The filled stippling in (a) and (b) indicates grid-cells with significant  
 137 deviations from JJA climatology using a significance test that accounts for the false discovery  
 138 rate (FDR) associated with multiple testing (9), while the grid-points marked with hollow  
 139 stippling indicate local significance.

140



141

142 **Figure 4. Recent trends in the occurrence of the wave 7 teleconnection.** (a) Number of  
 143 weeks per summer season (JJA) with wave 7 amplitude above average ( $>0\sigma$ ),  $1\sigma$  and  $1.5\sigma$   
 144 irrespective of phase position. (b) Number of weeks per summer season (JJA) where wave  
 145 seven is in its preferred phase position (see Fig. S3) and the amplitude of wave 7 is above  
 146 average ( $>0\sigma$ ),  $>1\sigma$  and  $>1.5\sigma$ .

147

148 **5 Conclusions**

149 It is important to note that extreme weather events such as the heatwaves observed in Summer  
150 2018 are the product of several factors acting together. For example it has been shown that the  
151 Extreme heatwaves in Europe 2003 and Russia 2010 were preceded by very low soil moisture  
152 content due to an anomalous dry spring season (10–12) and there is good reasons to believe  
153 that the anomalously dry April-May conditions in many parts of the NH contributed to a large  
154 degree to the magnitude and persistence of the observed heatwaves by known soil moisture  
155 feedbacks. In general, record breaking heat and rainfall extremes are the expected outcome of  
156 a warming mean climate due to increasing greenhouse gas (GHG) emissions (13, 14). GHG  
157 warming leads to more intense events heat and an enhanced water holding capacity of the air  
158 which fuels heavy rainfall. The timing, duration and location of a specific extreme weather  
159 event, however is largely controlled by the large scale circulation, especially in the mid-  
160 latitudes (15). While the direct response to thermodynamic drivers of weather extremes are  
161 generally well understood, large uncertainty remains when it comes to the indirect response  
162 via the changes in dynamical circulation drivers under a warmer climate (15–19). Changes in  
163 the dynamical circulation have been proposed to explain the increase in persistence and  
164 magnitude of recent summer extremes, that have exceeded what would be expected from  
165 simple thermodynamic arguments (19, 20), particularly in the case of Western and Central  
166 Europe as well as the Southern Central US being repeatedly struck by devastating heatwaves  
167 (12, 21–24). Summer storm tracks have been weakening over recent decades (25) which  
168 likely influences planetary wave behavior. In boreal summer Rossby waves have indeed been  
169 increasing recently in agreement with our results (26). Others however have shown that  
170 upward trends over a relatively short period are not statistically significant (27) and traditional  
171 blocking indices show no changes in summer (28). The regions for which an increase in the  
172 persistence of regional weather regimes was identified, however, (Northern US, Europe and  
173 Western Asia) match those related to the wave 7 teleconnection pattern (29). Planetary wave  
174 resonance has been discussed as a potential mechanism to generate high amplitude synoptic  
175 wave patterns in boreal summer (4, 8, 30) and required conditions were present in June July  
176 as well (also see discussion in SI). Recent trends in the zonal temperature profile due to  
177 anthropogenic climate change have been suggested to favour resonance conditions (31). This  
178 temperature profile bears imprints of enhanced land warming and high latitude warming and  
179 is associated with the formation of double-jets in the zonal mean zonal wind (8, 31). In the  
180 given case a double jet pattern was visible over the Eurasian continent (Fig. S9), which might  
181 be the reason that planetary wave patterns were specifically amplified and persistent.

182 In summary, we have shown that the summer 2018 featured a series of near simultaneous  
183 extreme weather events that coincided in time and space with a circumglobal teleconnection  
184 constituted by an amplified Rossby wave of wavenumber 7 in the mid-latitude jet stream.  
185 These extremes include the heat-records of June/July broken in North America, Western  
186 Europe and Caspian Sea region, as well as the extreme and devastating rainfall events in  
187 South-East Europe and Japan. Tropical ENSO variability in 2018 was in a neutral state and  
188 thus unlikely to be an important factor behind the extreme weather events in the NH. This  
189 recurrent circulation pattern conducive for heat waves acts in addition to the  
190 thermodynamically driven increase in heat, creating possibilities for very-extreme heat waves,

191 specifically in the identified regions: Western Europe, North America and Caspian Sea  
192 region. We show that this circumglobal teleconnection pattern has increased in frequency and  
193 persistence in recent years. Given the high impacts of these extremes in terms of mortality,  
194 morbidity and agricultural losses, this presents major risks for society and global food  
195 production in particular, since the main breadbasket regions are located in the mid-latitudes.  
196 Further research is required to fully understand the combination of factors that trigger these  
197 observed wave events, and what determines their preferred phase position, so that  
198 predictability of future extreme events can be improved.

199

## 200 **References:**

- 201 1. NOAA, “State of the Climate: Global Climate Report for July 2018” (2018), (available at  
202 <https://www.ncdc.noaa.gov/sotc/global/201807>).
- 203 2. NOAA, “State of the Climate: Global Climate Report for June 2018” (2018), (available at  
204 <https://www.ncdc.noaa.gov/sotc/global/201806>).
- 205 3. International Federation of Red Cross and Red Crescent Societies, “Information Bulletin no. 1  
206 Flash floods in Europe” (2018).
- 207 4. K. Kornhuber *et al.*, Summertime Planetary Wave-Resonance in the Northern and Southern  
208 Hemisphere. *J. Clim.* **30**, 6133–6150 (2017).
- 209 5. G. Branstator, Circumglobal Teleconnections, the Jet Stream Waveguide, and the North  
210 Atlantic Oscillation. *J. Clim.* **15**, 1893–1910 (2002).
- 211 6. G. Branstator, H. Teng, Tropospheric Waveguide Teleconnections and Their Seasonality. *J.*  
212 *Atmos. Sci.* **74**, 1513–1532 (2017).
- 213 7. J. Zhang, J. Yuanchun, C. Haishan, W. Zhiwei, Double-mode adjustment of Tibetan Plateau  
214 heating to the summer circumglobal teleconnection in the Northern Hemisphere. *Int. J.*  
215 *Climatol.* (2017), doi:10.1002/joc.5201.
- 216 8. K. Kornhuber, V. Petoukhov, S. Petri, S. Rahmstorf, D. Coumou, Evidence for wave resonance  
217 as a key mechanism for generating high-amplitude quasi-stationary waves in boreal summer.  
218 *Clim. Dyn.* **49**, 1961–1979 (2017).
- 219 9. D. Wilks, “the Stippling Shows Statistically Significant Grid Points .” *Bull. Am. Meteorol.*  
220 *Soc.* **97**, 2263–2274 (2016).
- 221 10. E. M. Fischer, S. I. Seneviratne, D. Lüthi, C. Schär, Contribution of land-atmosphere coupling  
222 to recent European summer heat waves. *Geophys. Res. Lett.* **34**, L06707 (2007).
- 223 11. D. G. Miralles, A. J. Teuling, C. C. van Heerwaarden, J. Vilà-Guerau de Arellano, Mega-  
224 heatwave temperatures due to combined soil desiccation and atmospheric heat accumulation.  
225 *Nat. Geosci.* **7**, 345–349 (2014).
- 226 12. E. Black, M. Blackburn, G. Harrison, B. Hoskins, J. Methven, Factors contributing to the  
227 summer 2003 European heatwave. *Weather.* **59**, 217–223 (2004).
- 228 13. J. Lehmann, D. Coumou, K. Frieler, Increased record-breaking precipitation events under  
229 global warming. *Clim. Change.* **132**, 501–515 (2015).
- 230 14. S. Rahmstorf, D. Coumou, Increase of extreme events in a warming world. *Proc. Natl. Acad.*  
231 *Sci. U. S. A.* **108**, 17905–9 (2011).



- 232 15. T. G. Shepherd, Atmospheric circulation as a source of uncertainty in climate change  
233 projections. *Nat. Geosci.* **7**, 703–708 (2014).
- 234 16. J. Cohen *et al.*, Recent Arctic amplification and extreme mid-latitude weather. *Nat. Geosci.* **7**,  
235 627–637 (2014).
- 236 17. E. A. Barnes, J. A. Screen, The impact of Arctic warming on the midlatitude jet-stream: Can it?  
237 Has it? Will it? *Wiley Interdiscip. Rev. Clim. Chang.* (2015) (available at  
238 <http://doi.wiley.com/10.1002/wcc.337>).
- 239 18. B. Hoskins, T. Woollings, Persistent Extratropical Regimes and Climate Extremes. *Curr. Clim.*  
240 *Chang. Reports.* **1**, 115–124 (2015).
- 241 19. R. M. Horton, J. S. Mankin, C. Lesk, E. Coffel, C. Raymond, A Review of Recent Advances in  
242 Research on Extreme Heat Events. *Curr. Clim. Chang. Reports.* **2**, 242–259 (2016).
- 243 20. J. Luterbacher *et al.*, European Seasonal and Annual Temperature Variability, Trends, and  
244 Extremes Since 1500. *Science (80-. )*. **303**, 1499–1503 (2004).
- 245 21. A. Hoy, S. Hänsel, P. Skalak, Z. Ustrnul, O. Bochníček, The extreme European summer of  
246 2015 in a long-term perspective. *Int. J. Climatol.*, 1–20 (2016).
- 247 22. M. Rebetez, O. Dupont, M. Giroud, An analysis of the July 2006 heatwave extent in Europe  
248 compared to the record year of 2003. *Theor. Appl. Climatol.* **95**, 1–7 (2009).
- 249 23. M. Hoerling, J. K. Eischeid, X. Quan, T. Xu, Explaining the record US warmth of 2006.  
250 *Geophys. Res. Lett.* **34**, 1–4 (2007).
- 251 24. N. S. Diffenbaugh, M. Scherer, Likelihood of July 2012 U.S. temperatures in preindustrial and  
252 current forcing regimes. *Bull. Am. Meteorol. Soc.*, 6–9 (2013).
- 253 25. D. Coumou, J. Lehmann, J. Beckmann, The weakening summer circulation in the Northern  
254 Hemisphere mid-latitudes. *Science (80-. )*. **348**, 324–327 (2015).
- 255 26. S.-Y. Wang, R. E. Davies, R. R. Gillies, Identification of extreme precipitation threat across  
256 midlatitude regions based on short-wave circulations. *J. Geophys. Res. Atmos.* **118**, 11059–  
257 11074 (2013).
- 258 27. J. A. Screen, I. Simmonds, Exploring links between Arctic amplification and mid-latitude  
259 weather. **40**, 959–964 (2013).
- 260 28. T. Woollings *et al.*, Blocking and its Response to Climate Change. *Curr. Clim. Chang.*  
261 *Reports*, 1–14 (2018).
- 262 29. D. E. Horton *et al.*, Contribution of changes in atmospheric circulation patterns to extreme  
263 temperature trends. *Nature.* **522**, 465–469 (2015).
- 264 30. V. Petoukhov, S. Rahmstorf, S. Petri, H. J. Schellnhuber, Quasiresonant amplification of  
265 planetary waves and recent Northern Hemisphere weather extremes. *Proc. Natl. Acad. Sci.* **110**,  
266 5336–41 (2013).
- 267 31. M. E. Mann *et al.*, Influence of Anthropogenic Climate Change on Planetary Wave Resonance  
268 and Extreme Weather Events. *Sci. Rep.* **7**, 45242 (2017).

269

270

271

272

273 **Acknowledgements:**

274 We thank the European Centre for Medium Range Weather Forecasts (ECMWF) for access to their  
275 Operational Analysis data and the federal state of Brandenburg is acknowledged for supporting the  
276 used high-performance computing resources. **Funding:** This work was supported by the UK Natural  
277 Environment Research Council (NERC) National Centre for Atmospheric Science (NCAS) and NERC  
278 grants NE/P006779/1 and NE/N018001/1 (K.K., L.G. and S.O.) and by the German Federal Ministry of  
279 Education and Research (BMBF) and by the Netherlands Organisation for Scientific Research (NWO)  
280 (D.C). **Author contributions:** K.K., S.O., D.C., L.G. conceptualised the paper. K.K. undertook the  
281 analysis. All authors contributed to the writing of the paper. **Competing Interests:** The authors  
282 declare no competing interests. **Data and materials availability:** The data used in this study can be  
283 obtained from the ECMWF and NCEP-NCAR websites or via the UK Centre for Environmental Data  
284 Analysis (CEDA)

285

1  
2  
3  
4  
5  
6  
7  
8  
9  
10  
11  
12  
13  
14  
15  
16  
17  
18  
19  
20  
21  
22  
23  
24

Supporting Information for

**Extreme weather events in early summer 2018 connected by a recurrent hemispheric wave pattern**

Kai Kornhuber <sup>1,2\*</sup>, Scott Osprey <sup>1,2</sup>, Dim Coumou <sup>3,4</sup>, Stefan Petri <sup>3</sup>,  
Vladimir Petoukhov <sup>3</sup>, Stefan Rahmstorf <sup>3</sup>, Lesley Gray <sup>1,2</sup>

<sup>1</sup>Atmospheric, Oceanic and Planetary Physics, University of Oxford, Oxford, United Kingdom

<sup>2</sup>National Centre for Atmospheric Science, United Kingdom

<sup>3</sup>Earth System Analysis, Potsdam Institute for Climate Impact Research, Potsdam, Germany

<sup>4</sup>Institute for Environmental Studies, Vrije Universiteit Amsterdam, Amsterdam, Netherlands

\*Corresponding author: kai.kornhuber@physics.ox.ac.uk

25 **Contents of this file**

26 Text S1 to S2

27 Figures S1 to S9

28 Tables S1 to S2

29 **Text S1. Japanese Floods early July 2018.**

30 From late June through to early July the slow-moving circulation identified over Eurasia coincided  
31 with large high-pressure systems north and east of Japan (Fig. S1). This confined a north-east flow of  
32 warm moist air over Japan from lower latitudes. At the same time a seasonally stalled Meiyu weather  
33 front stretched across Japan causing persistent rainfall in the south-west Okinawa prefecture . These  
34 persistent rains were further exacerbated by the passage of ex-tropical storm Prapiroon over the  
35 affected areas, causing major flooding. A meandering atmospheric river of high moisture laden air is  
36 clearly evident in Fig. S1a at the time of this flooding event, which is clearly influenced by the  
37 background slow moving circulation patterns seen in Fig. S1b.

38

39 **Text S2. Quasi-resonant amplification during June-July 2018.**

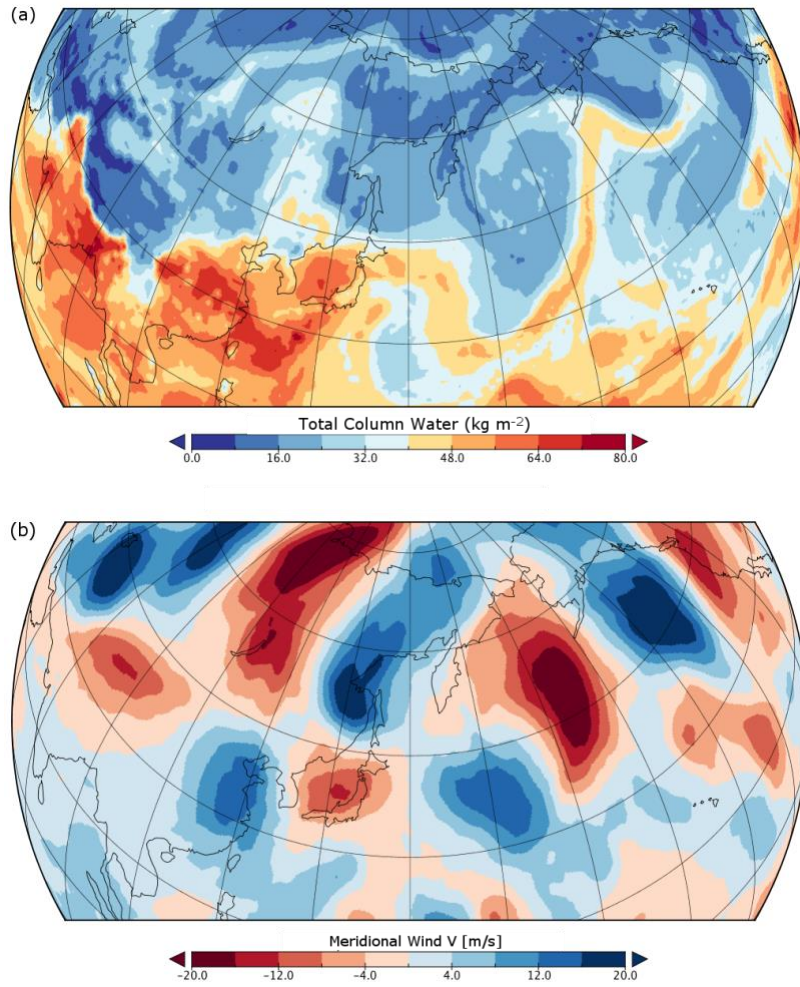
40

41 Quasi-resonant amplification (QRA) was proposed as a dynamical mechanism that could lead to the  
42 high-amplitude planetary waves of synoptic scale wavenumbers 6-8 (4–6). The QRA mechanism as  
43 derived by Petoukhov et al. (4) assumes that ‘a synoptic-scale free wave trapped in a midlatitude  
44 waveguide can resonate with the slow-moving forced wave and thereby increase its amplitude  
45 through a quasi-resonant amplification’ (6). This framework thus differs from the concept of  
46 ‘resonance’ described in Held 1983(12) as waves are not assumed to encircle the longitudinal belt to  
47 interact with the “tails” of themselves (also see our reply to comment 1). The theory behind this  
48 mechanism is based on linear theory, and assumes a zonally symmetric background flow on which  
49 perturbations develop (7, 13) but it only considers zonally elongated waves (in contrast to e.g.  
50 Hoskins & Karoly (7) who discuss meridionally propagating waves). It describes similar phenomena as  
51 Branstator et al. (8, 9) who showed that circumglobal wave patterns can evolve when a waveguide is  
52 provided in zonal direction by a mid-latitude jet. A zonal waveguide effectively traps those waves  
53 in the mid-latitudes, preventing their dissipation in the meridional direction, which is the first  
54 precondition for QRA.

55

56 We tested the resonance conditions (Table S2) for the 2018 summer following the methodology of  
57 (2) (see Table S2 for details). Figure S8 provides evidence that the persistent wave 7 circulation  
58 pattern is consistent with the resonance of atmospheric waves trapped in a mid-latitude waveguide.  
59 It shows the time evolution of the prime quantities associated with wave resonance: The zonally  
60 averaged zonal wind  $U$  as a measure for the background flow (Fig. S8a), the squared meridional  
61 wavenumber ( $l^2$ ) that determines waveguide formation (Fig.S8b) which is critical for resonance  
62 detection (Fig. S8c). A ‘double jet’ in the zonal mean jet evolves in early June (i.e. two peaks in  $U$  at  
63  $\sim 45N$  and  $75N$ ). This configuration in the zonal mean zonal wind is characterized by a narrow  
64 subtropical jet with sharp edges which is known to favor waveguides (14). Figure S9 shows a 15-day  
65 average of the zonal wind field centered around the 1st July 2018. The zonal winds form a near  
66 circumglobal jet, which splits into a double jet configuration at  $15W$  over Eurasia. A waveguide forms  
67 for wave 7 as indicated by the two turning points in  $l^2$  (dotted black lines in Fig. S8b). The detection  
68 scheme also indicates sufficient orographic / thermal forcing and therefore resonance is detected  
69 from mid-June onwards (Fig. 2b, S8c). As expected from resonance theory (4), a few days later the  
70 phase speed of wave 7 slows down and the amplitude increases to a level above 1.5 standard  
71 deviations (Fig. 2d, e).

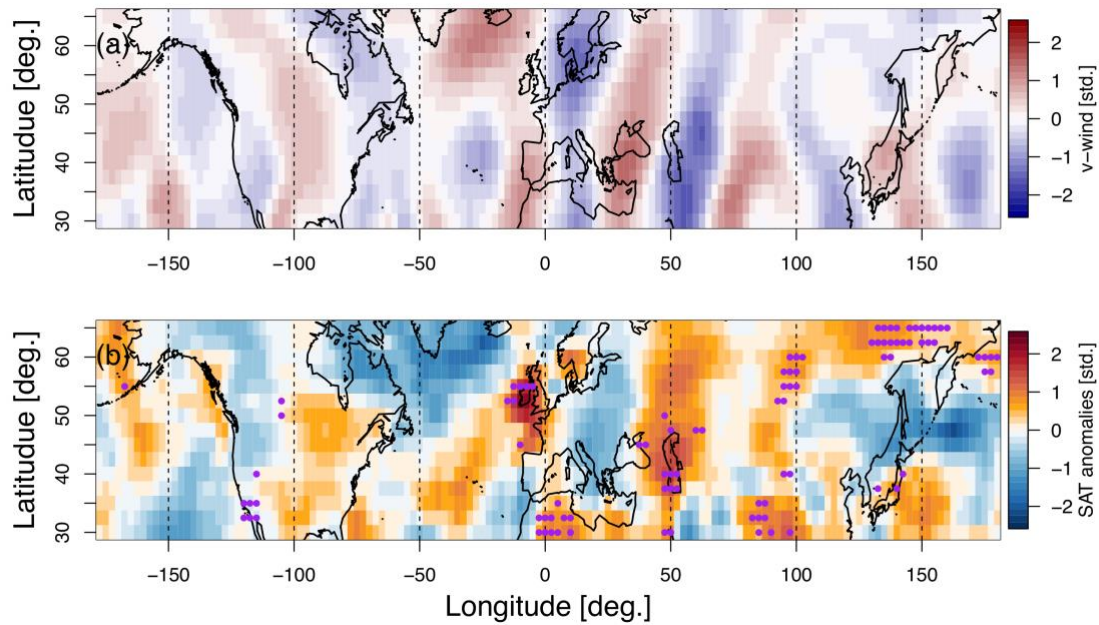
72



73

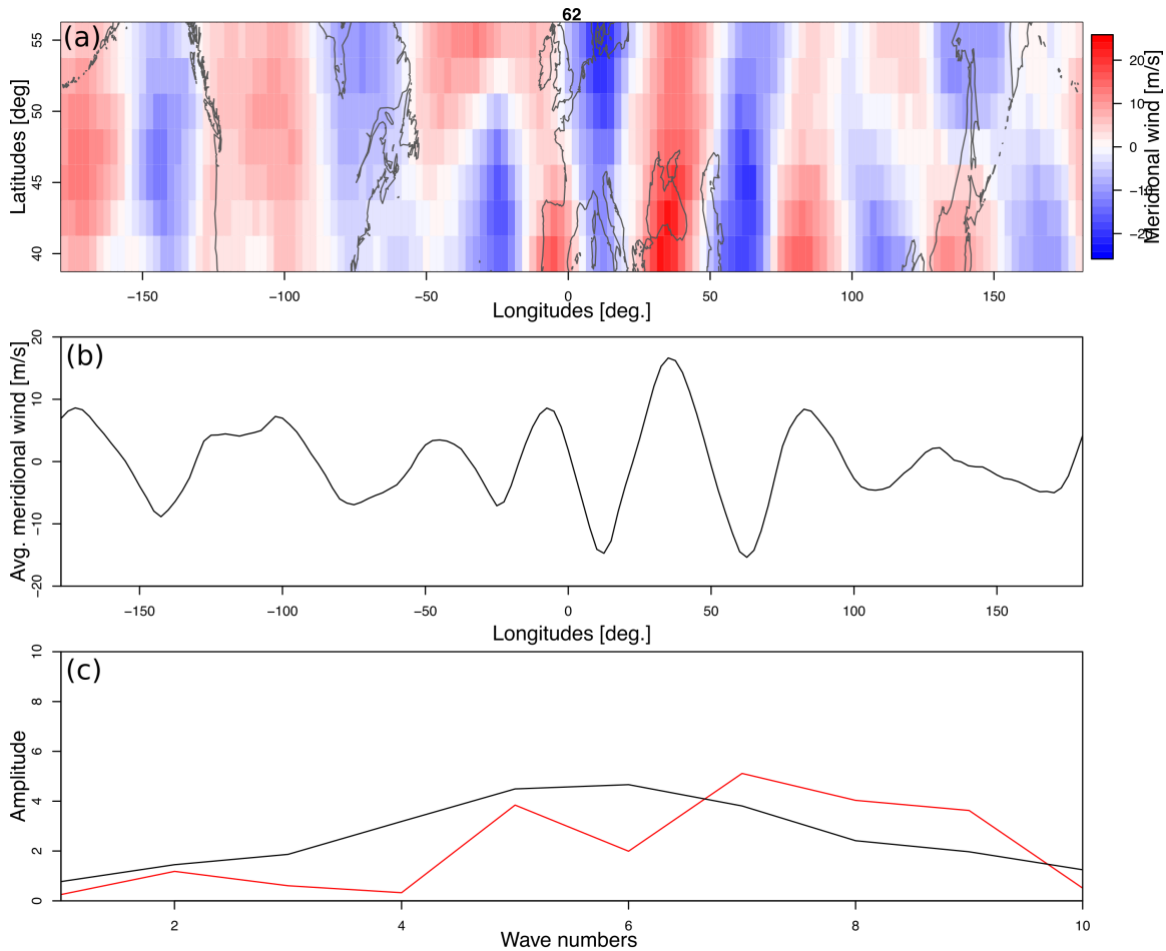
74 **Figure S1. The role of the large-scale circulation in the Japanese Floods 2018. (A) Total column**  
75 **water measured 4th of July over the East Asian Pacific Sector (B) Meridional windspeeds centered on**  
76 **4th July (7-day running average).**

77

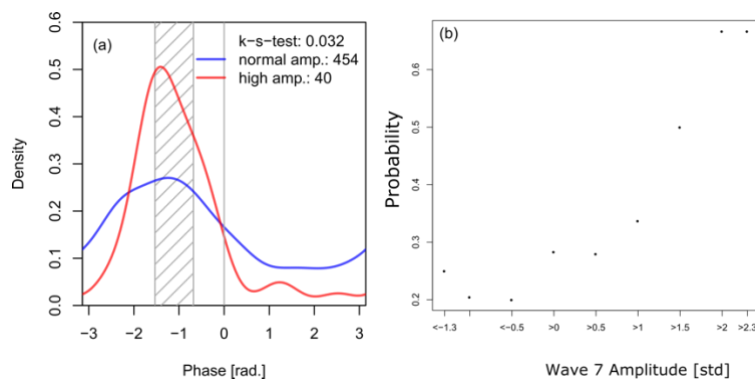


78  
 79 **Figure S2. Meridional winds and surface temperature anomalies in units of standard deviation.** (a)  
 80 15-day average of daily anomalies in units of standard deviation centered around the 1st of July  
 81 2018. The meridional winds are arranged in form of a circumglobal wave pattern specifically in the  
 82 mid-latitude belt (30N- 55N). (b) Same as in (a) but for linearly detrended temperature anomalies.  
 83 Temperature anomalies occur in line with the position of ridges and troughs of the circumglobal  
 84 wave pattern depicted in (b), reaching values of above 2 std. in Europe and above 1 std. in Central  
 85 US, the Caspian Sea region, Northern China, Siberia and Japan. Grid-points that exhibit daily record  
 86 temperatures within the 15-day window around the 1st of July are marked by purple dots. Those  
 87 grid-points agree well with the regions marked in Fig.2 in the main manuscript.

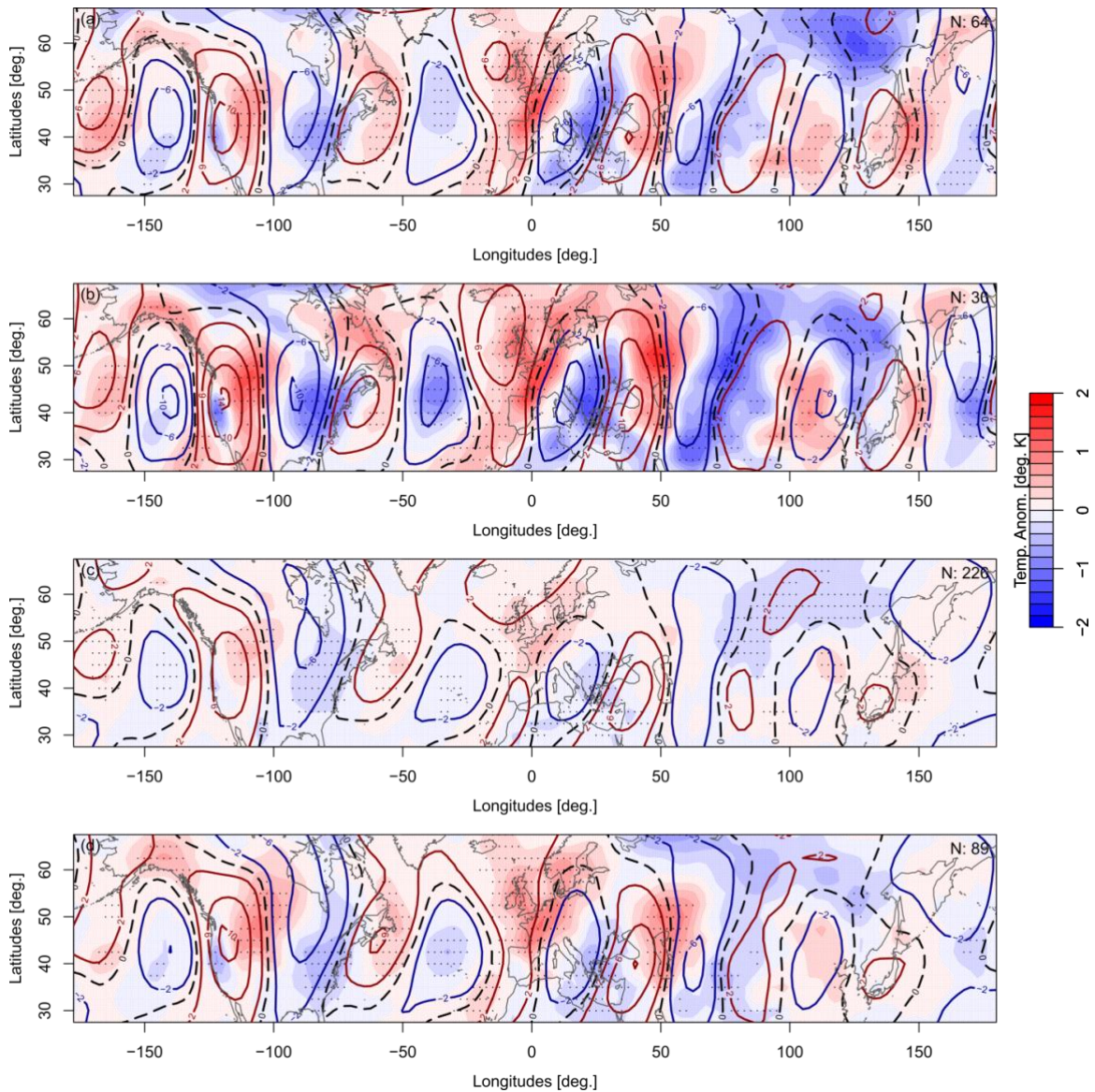
88



89 **Figure S3. A circumglobal wave pattern during Jun-July 2018.** (a) Meridional winds (15 day mean  
 90 centered around the 1. Of July). (B) the meridional averaged meridional winds in the mid. latitudinal  
 91 belt (37.5N-57.5N). (c) Rossby wave amplitudes of wavenumbers 1-10 determined by applying a Fast-  
 92 Fourier-Transformation on the data shown in (b).  
 93  
 94

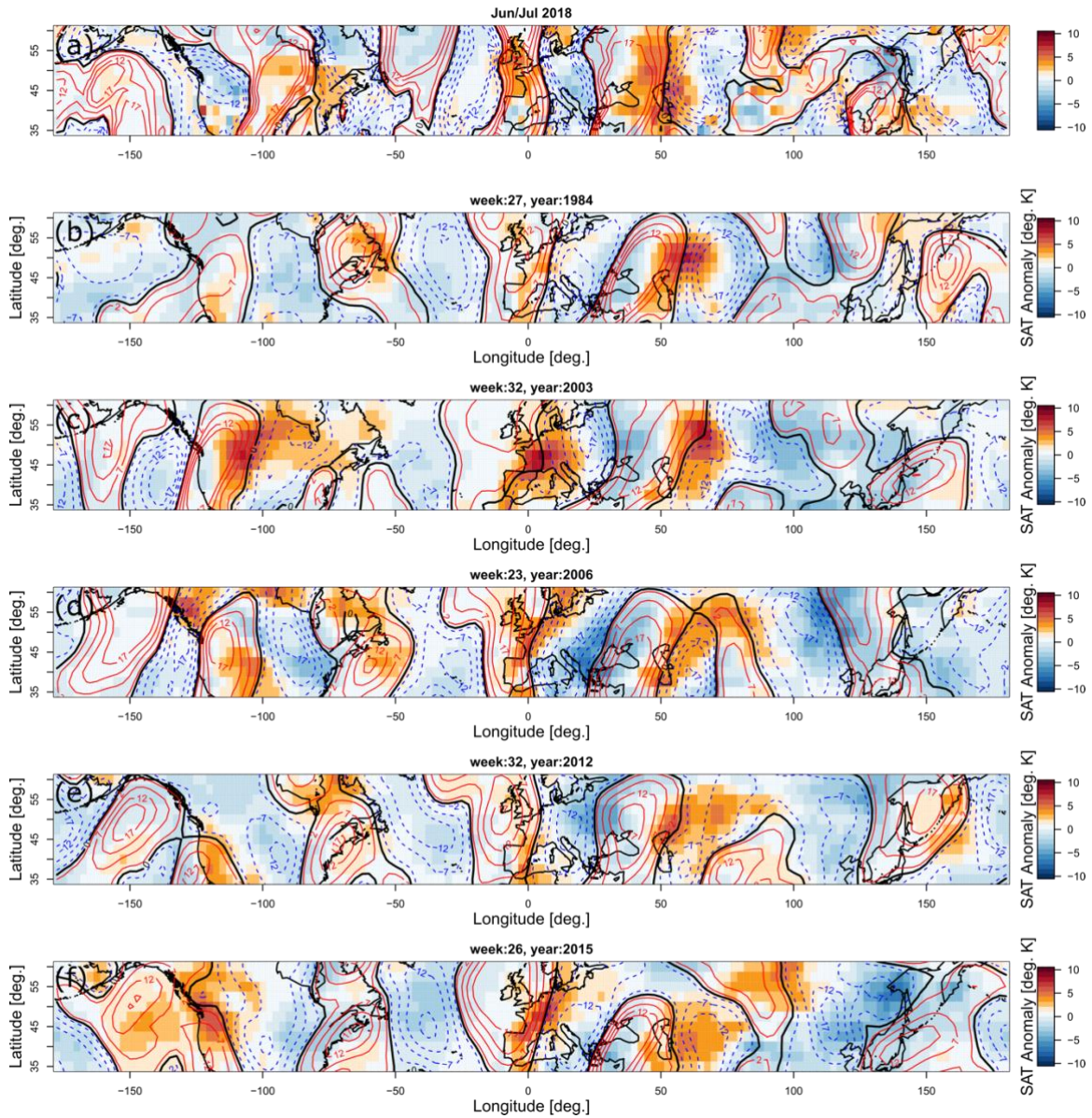


95 **Figure S4. Evidence for a circumglobal wave 7 Teleconnection.** (a) Probability density distributions  
 96 during summer (JJA), comparing weeks of high amplitude ( $> 1.5\sigma$ , red) and normal amplitude ( $< 1.5\sigma$ ,  
 97 blue) of wave 7 (b) Probability of a week in summer (JJA) to exhibit phase of wavenumber 7 within  
 98 the phase locked region as defined by the 25th -75th percentile of the high amplitude wave 7 ( $>$   
 99  $1.5\sigma$ ). The probability increases with amplitude of wave 7.  
 100



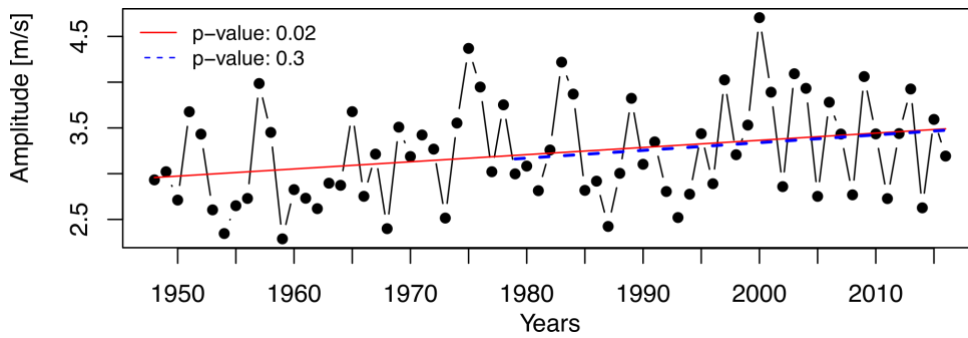
101  
 102 **Figure S5. The recurrent wave-7 teleconnection.** Composite temperature anomalies (filled contours)  
 103 and meridional wind velocities (southward: red line contour, northward: blue line contour, zero wind  
 104 line: black line) during weeks of wave-7 amplitude in summer (JJA, 1979 – 2016) **(a)** within the  
 105 preferred phase position (see Fig.S3a, phase locked from here on) and above average, **(b)** phase  
 106 locked and above  $1\sigma$ , **(c)** above average irrespective of phase position, **(d)** above  $1\sigma$  irrespective of  
 107 phase position. Continental coastlines are depicted by grey outlines. The respective number N of  
 108 averaged weeks is given in the upper right corner. Grey dots mark the grid-points where anomalies  
 109 are significantly different (95% confidence level) from the remaining weeks. Note that unlike in Fig.  
 110 3a,b shown in the manuscript no false discovery rate significance testing (FDR(2)) was applied here.  
 111





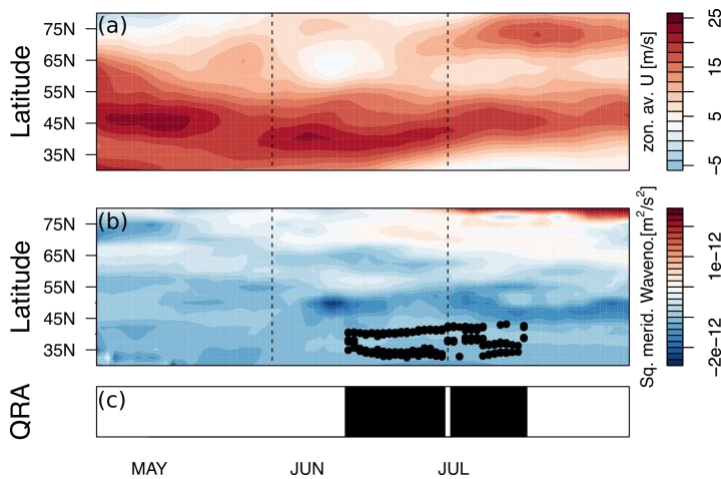
112  
 113 **Figure S6. Hemispheric temperature and circulation extremes over the recent past. (a)** Surface  
 114 surface temperature anomalies (compared to 1981-2010 climatology, filled contours) and meridional winds  
 115 (line contours, North-South: blue, South-North: red) in a 15-day running-mean centered around 1  
 116 July. **(b-f)** Same variables shown during selected examples of this pattern observed during summers  
 117 of severe heatwaves in the Northern Hemisphere based on weekly means, including the severe  
 118 European heatwaves of **(c)** 2003 and **(f)** 2015. For a full list see table S1.

119  
 120  
 121  
 122  
 123  
 124



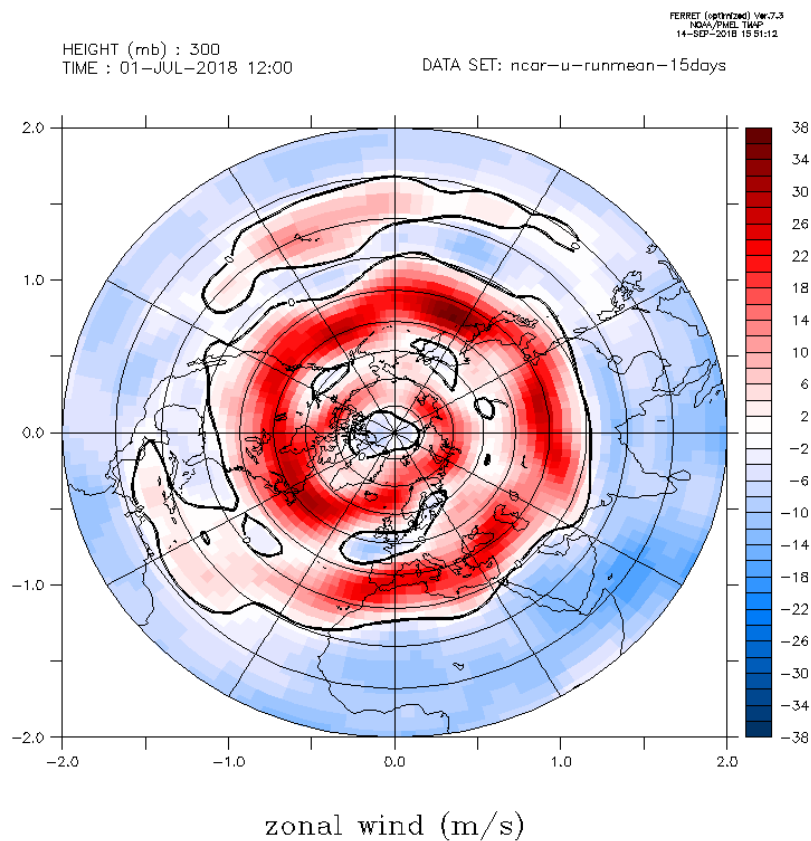
125  
126  
127  
128  
129  
130  
131  
132

**Figure S7. Long term trends in wave 7 amplitude.** Mean wave 7 amplitude in summer (June-August) from over the period 1948 – 2016. Linear trends for the entire period (red solid line) statistically significant but might be spurious due to changes in measurement systems. Trends over the satellite-based measurement period (1979-2016) increasing but are not significant.



133  
134  
135  
136  
137  
138  
139  
140

**Figure S8. Resonance detection of wavenumber 7 early Summer 2018.** (a) Time-series of zonally averaged zonal wind. A ‘double jet pattern’ forms at the beginning of June in the zonal mean. (b) Squared meridional wavenumber. A waveguide, the key condition for wave resonance, forms in the mid-July for wavenumber 7, as shown by the black dots. (c) Resonance is detected from mid-July on (marked in black).



141  
142

143 **Figure S9. Zonal wind component in the upper troposphere.** Shown is the 15-day mean, centered on  
144 July 1st 2018. A strong subtropical jet is visible over the entire longitudinal belt which splits into a  
145 double jet pattern over the Eurasian continent at about 15°W. The jet shows positive values around  
146 the entire hemisphere, thus providing a waveguide which can be considered circumglobal.

147  
148

149

150

151

152

153

154

155

156

157

158

159

Year	Month	First day of week
1979	6	29
1980	6	1
1983	7	6
1983	7	13
1984	6	15
1985	6	29
1988	6	29
1989	6	15
1989	7	13
1989	7	27
1991	8	17
1995	7	6
1996	7	13
1997	6	1
1997	8	24
1998	8	3
2000	6	29
2000	7	20
2001	6	22
2003	7	6
2003	7	13
2003	8	3
2003	8	10
2004	7	13
2005	6	15
2006	6	1
2006	6	8
2009	6	1
2009	6	22
2009	6	29
2010	6	8
2010	6	29
2010	7	6
2012	6	22
2012	8	10
2013	6	22
2013	6	29
2015	6	29
2015	8	10
2015	8	24

160

161 **Table S1. Dates of weeks with wave number 7 above  $1.5\sigma$ , as used in the analysis shown in Fig. 3 a,**  
 162 **b.**

163

<b>i. Waveguide for synoptic scale free wave <math>k</math>:</b>
1. Two turning points (TPs, change of sign) in $l^2$
2. $l^2 > 0$ between the turning points (TP)
3. $U > 0$ in between and in the vicinity of the TPs
4. The highest value of $l^2$ between the TPs is in the range of $l_{min}^2$ and $l_{max}^2$
5. The TPs lie within a region of 30°N and 70°N
6. The TPs have a minimum distance of $w_k$
7. In case of two waveguides their distance has to exceed at least 5°
<b>ii. Effective Forcing Amplitude for forced planetary wave <math>m \approx k</math>:</b>
8. The effective forcing Amplitude $A_{eff}$ for a respective wave number $m$ has to exceed a certain threshold $q_k$ , defined by the 50 <sup>th</sup> percentile of the overall wave spectrum on a specific timestep.

164 **Table S2. Key Conditions for resonance detection from (10)**

165  
166  
167  
168  
169  
170

171 **References:**

- 172 1. Kalnay, The NCEP/NCAR 40-year reanalysis project. Bull. Am. Meteorol. Soc., 437–470 (1996).
- 173 2. D. Wilks, “ the Stippling Shows Statistically Significant Grid Points .” Bull. Am. Meteorol. Soc. 97,  
174 2263–2274 (2016).
- 175 3. D. Coumou, V. Petoukhov, S. Rahmstorf, S. Petri, H. J. Schellnhuber, Quasi-resonant circulation  
176 regimes and hemispheric synchronization of extreme weather in boreal summer. Proc. Natl. Acad.  
177 Sci. 111, 12331–12336 (2014).
- 178 4. V. Petoukhov, S. Rahmstorf, S. Petri, H. J. Schellnhuber, Quasiresonant amplification of planetary  
179 waves and recent Northern Hemisphere weather extremes. Proc. Natl. Acad. Sci. 110, 5336–41  
180 (2013).
- 181 5. V. Petoukhov et al., Role of quasiresonant planetary wave dynamics in recent boreal spring-to-  
182 autumn extreme events. Proc. Natl. Acad. Sci. 113, 6862–6867 (2016).
- 183 6. K. Kornhuber et al., Summertime Planetary Wave-Resonance in the Northern and Southern  
184 Hemisphere. J. Clim. 30, 6133–6150 (2017).
- 185 7. B. J. Hoskins, D. J. Karoly, The Steady Linear Response of a Spherical Atmosphere to Thermal and  
186 Orographic Forcing. J. Atmos. Sci. 38, 1179–1196 (1981).
- 187 8. G. Branstator, H. Teng, Tropospheric Waveguide Teleconnections and Their Seasonality. J. Atmos.  
188 Sci. 74, 1513–1532 (2017).

- 189 9. G. Branstator, Circumglobal Teleconnections, the Jet Stream Waveguide, and the North Atlantic  
190 Oscillation. *J. Clim.* 15, 1893–1910 (2002).
- 191 10. K. Kornhuber, V. Petoukhov, S. Petri, S. Rahmstorf, D. Coumou, Evidence for wave resonance as a  
192 key mechanism for generating high-amplitude quasi-stationary waves in boreal summer. *Clim. Dyn.*  
193 49, 1961–1979 (2017).
- 194 11. L. Stadherr, D. Coumou, V. Petoukhov, S. Petri, S. Rahmstorf, Record Balkan floods of 2014 linked  
195 to planetary wave resonance. *Sci. Adv.* 2, e1501428 (2016).
- 196 12. V. Petoukhov et al., The role of quasi-resonant planetary wave dynamics in recent boreal spring-  
197 to-autumn extreme events. *Proc. Natl. Acad. Sci.* 113, 6862–6867 (2016).
- 198 13. I. M. Held, (Academic Press, London, 1983), pp. 127–168.
- 199 14. I. Manola, F. Selten, H. De Vries, W. Hazeleger, “Waveguidability” of idealized jets. *J. Geophys.*  
200 *Res. Atmos.* 118, 10432–10440 (2013)

